Headline Articles

Atomic-Scale Surface Structures of TiO_2 (110) Determined by Scanning Tunneling Microscopy: A New Surface-Limited Phase of Titanium Oxide

Hiroshi Onishi, Ken-ichi Fukui, and Yasuhiro Iwasawa*

Department of Chemistry, Graduate School of Science, The University of Tokyo, Hongo, Bunkyo-ku, Tokyo 113

(Received February 14, 1995)

The structure transformation of a TiO_2(110) surface was observed at atomic-scale resolution by scanning tunneling microscopy (STM) and low-energy electron diffraction (LEED). Irregular corrugations on an argon-bombarded TiO_2(110) surface crystallized to stacked (1×1) terraces by vacuum annealing at 600—800 K. The terraces grew in dimension to be as large as 30×30 nm^2 at 900 K. The unoccupied surface states localized on individual Ti^{4+} ions were resolved on a (1×1) terrace. The position of the Ti^{4+} ions was probed by imaging adsorbed formate ions. Annealing at higher temperatures resulted in the formation of a wide row structure comprising double strands. Imaging of individual adsorbed formate ions was used to grade possible structure models by probing Ti ions exposed on the surface; thereby, an added Ti_2O_3 row model, which is a new surface-limited phase of titanium oxide consisting of Ti^{3+} ions of the optimum six-fold coordination, was concluded for the double-strand structure. These results demonstrate the ability of probing experiments with an adsorbed molecule to determine the chemical nature of imaged sites on multi-component materials by STM.

Scanning tunneling microscopy (STM) has been bringing novel insights concerning surface chemistry on metals and semiconductors.[1,2] The decomposition reaction of adsorbed ethene was monitored on Pt(111).[3] It was suggested that hydrogen adsorption promoted the formation of NiH_x chains on Ni(110).[4] The formation of an oxidized chain was observed on Cu(110), where mobile copper atoms migrated on the terrace, even at room temperature, being oxidized into –O–Cu–O– chains.[5] On Si(111)-(7×7), the diffusion of vacancies governed the Si transport in oxidative etching and oxide formation reactions.[6] Those pioneering results demonstrate that the kinetics of surface reactions can be observed in-situ by STM at an atomic-scale resolution. There are, however, limited STM results reported concerning metal-oxide surfaces, though metal oxides are fundamental materials for catalysts, gas sensors, ceramics, and dielectric or superconducting materials used for electronic devices. Very recently, atomically resolved images have been reported for TiO_2(110),[7—13] TiO_2(100)-(1×3),[14] $SrTiO_3$(100)-($\sqrt{5}\times\sqrt{5}$),[15,16] Fe_3O_4(100),[17] $Rb_{1/3}WO_3$(0001),[18] $Mo_{18}O_{52}$(100),[19] V_2O_5(010),[20,21] and a FeO_x-film prepared on Pt(111).[22] However, the chemical nature of the imaged sites was not always obvious on those multi-component surfaces.

In the present paper we report on atomic-scale imaging of a TiO_2(110) surface, including stacked (1×1) terraces and a partially reduced (1×2) reconstruction, extending our previous communication.[11] The transformation in the surface structure was observed with increasing annealing temperature. Titanium ions exposed on the surface were probed by imaging adsorbed formate ions. Thereby, a one-dimensional row of Ti^{4+} ions was found on the (1×1) surface, while a reconstruction with an added Ti_2O_3 row, where no titanium ion was exposed, was concluded on the (1×2) surface.

Rutile TiO_2 is a typical transition metal oxide used for catalysts, gas sensors, and electrodes in photoelectrolysis cells. Surface reactions play a crucial role in those applications. TiO_2 also provides an interesting field of surface chemistry. It has been thought that the local coordination environment dominates the reactions on a TiO_2 surface.[23] Structure-sensitive coupling reactions of adsorbed acetates[24] and formates[25] were found on a TiO_2 single-crystal surface. In the catalytic

decomposition reaction of formic acid on a $TiO_2(110)$ surface, we found that a switchover of the reaction paths from dehydration to dehydrogenation by the second reactant molecule; an adsorbed formate ion unimolecularly decomposed to CO and an adsorbed hydroxyl group ($HCOO^-(a) \rightarrow CO + OH^-(a)$), while the intermediate reacted with a formic acid molecule to yield CO_2 and dihydrogen ($HCOO^-(a) + HCOOH \rightarrow CO_2 + H_2 + HCOO^-(a)$).[26,27] It is thus interesting to trace the microscopic kinetics of chemical reactions on a TiO_2 surface by STM, and to consider the reactivity on the basis of the microscopic structures of reaction sites.

The (110) surface of rutile TiO_2 is regarded as being a stable truncation, whereas (001)[28] and (100)[29] surfaces reconstructed by vacuum annealing are considered to diminish the population of unstable four-fold coordinated Ti ions. Figure 1 illustrates the model proposed for the stoichiometric $TiO_2(110)$-(1×1) truncation.[30] A medium-energy backscattered electron diffraction (MEED) study supported the model.[31] The model contains two types of in-plane Ti ions: five-fold and six-fold coordinated. Protruding oxygen ions bridge the six-fold coordinated Ti ions, forming regular O-ridges along the [001] axis. The alternative alignment of the exposed, five-fold coordinated Ti-row, and the bridging O-ridge results in the characteristic anisotropy on this surface. One-dimensional transport was found in the migration of adsorbed formate ions along the Ti-row.[32]

Several STM studies were performed on $TiO_2(110)$ in air[33] and UHV.[7—13] Early studies[7—9] reported regular rows oriented along the $[\bar{1}13]$ or $[1\bar{1}1]$ direction on vacuum-annealed (1×1) surfaces, and assigned the $[1\bar{1}1]$-row to a crystallographic shear (CS) structure of partially reduced crystals. The CS model, however, failed to reproduce the (1×1) periodicity. Recently, ridges parallel to the [0 0 1] axis were found to cover the surface, corresponding to the (1×1) order.[10—13] Another feature, a protruding double-strand row along the [0 0 1] direction, was also reported and associated with a (1×2) reconstruction in the recent studies. Contradictory models have been proposed for the double-strand row.[10,11,13,34] Furthermore, an additional structure having a local $c(2\times1)$[10] or (2×2) symmetry[13] was observed on the surface by exposure to an oxygen ambient[10] or by further annealing in vacuum.[13] In the present study, the chemical nature of the (1×1) ridge and the double-strand row is examined.

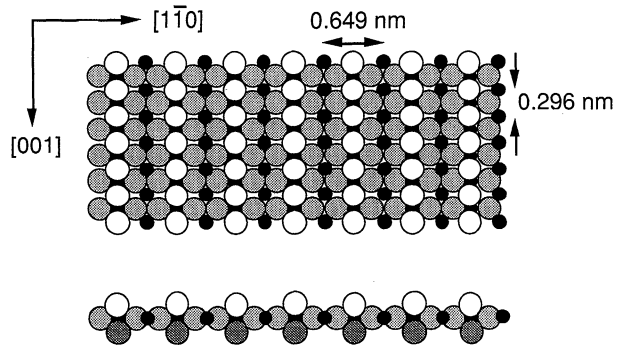

Fig. 1. A stoichiometric model of the $TiO_2(110)$-(1×1) surface. Filled and shaded symbols represent Ti^{4+} and O^{2-}, respectively. Plan and side views are shown.

Experimental

The experiments were carried out in an UHV-STM system (JEOL, JSTM4500VT, Japan) equipped with an Ar^+ gun and LEED-AES optics. The base pressure was 8×10^{-9} Pa. A polished $TiO_2(110)$ wafer of $6.5\times1\times0.25$ mm^3 (Earth Chemicals Co., Ltd., Japan) was annealed in air at 1100 K for 1 h. Nickel film was then deposited on a side of the wafer to resistively heat the crystal in the vacuum chamber. A small electrical input (ca. 2 V, 1 A) was sufficient to heat the wafer at 1200 K. The temperature of the surface was monitored with an IR radiation thermometer (Chino, IRFBP, Japan).

STM images were recorded at room temperature with a Pt–Ir tip. Positive sample bias voltages (V_s) of 0.5—2.0 V, and tunneling currents (I_t) of 0.2—0.3 nA were applied, while an opposite bias resulted in an unstable tunneling junction. A constant-current mode or a variable-current mode was employed in the imaging. In the latter mode, the z-position of the tip was controlled by a feedback loop with a larger time constant than in the former mode; thus, the surface topography was presented by small deviations in the tunneling current around a set value. Corrugations were presented as if they were illuminated from left side in the variable-current images shown below. This method of imaging was suitable for a rough or terraced surface. The dimensions of the imaged structure were determined in constant-current scans. The topography was presented in a gray scale in constant-current images. The scaling of the microscope was calibrated on a Si(111)-(7×7) surface.

In formate adsorption measurements, the TiO_2 surface was exposed to DCOOD (Merck, USA) at room temperature prior to STM observations. A capillary gas doser transported the reactant to the sample surface, thus minimizing contamination in the chamber. DCOOD was used to avoid H_2 background in thermal desorption and reaction experiments.[26,27]

Results and Discussion

Surface Preparation and Stoichiometry. A well-ordered (1×1) surface was prepared by cycles of argon bombardment (3 keV, 0.3 μA, 5 min) and vacuum annealing at 900 K (0.5—3 min). A sharp (1×1) LEED pattern was observed, and no impurity on the surface was detected by Auger electron spectroscopy (AES). The wafer became deep blue after tens of cleaning cycles. Argon sputtering and high-temperature annealing caused a deficiency in the oxygen concentration.[30] The following experiments were performed on the blue crystal with a resistivity of 2 Ω m. Assuming that the carrier density is inversely proportional to the resistivity, a slight deviation from the stoichiometry (−0.001%) was estimated for our wafer.[35] A carrier density of 6×10^{25}

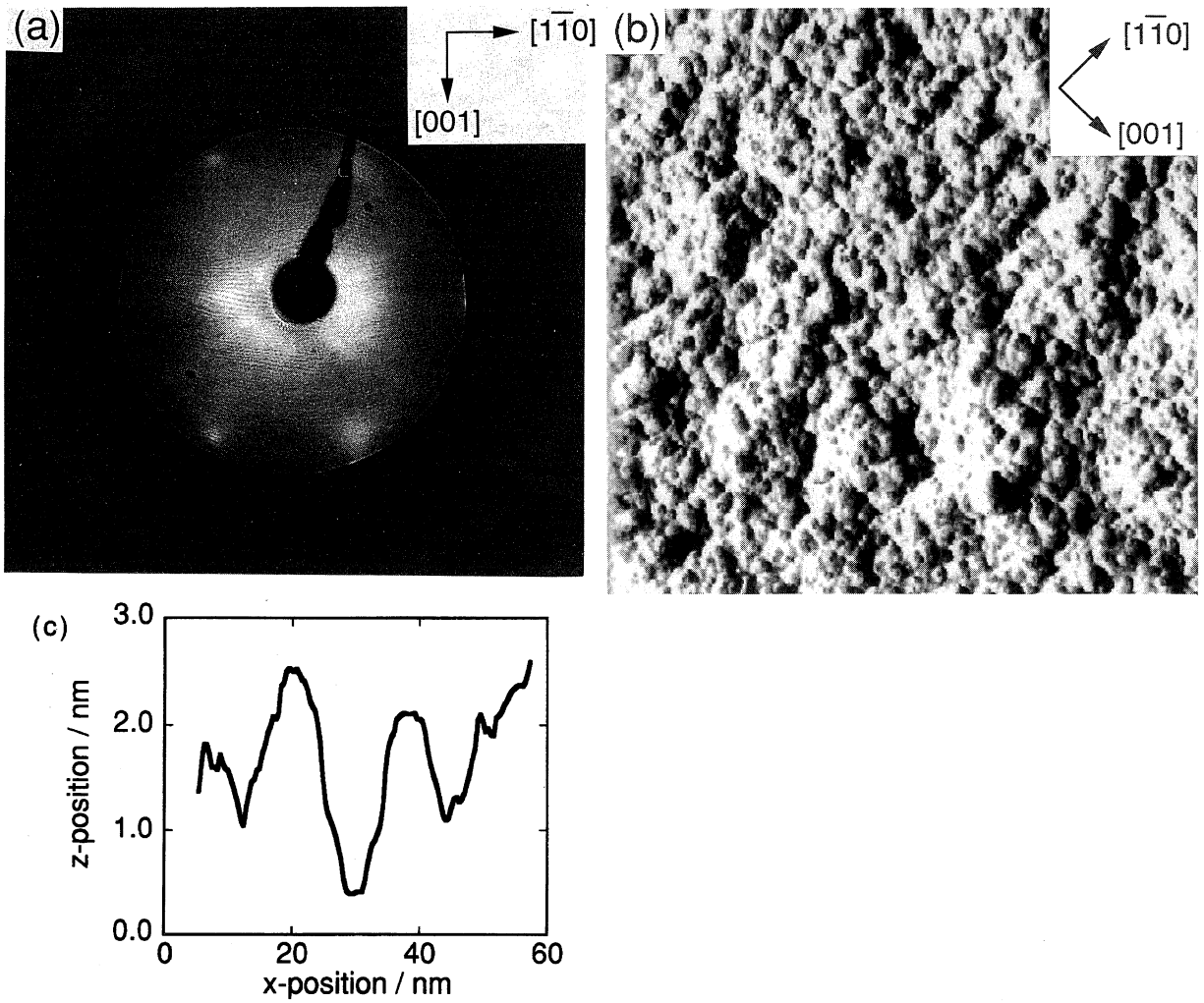

Fig. 2. LEED and STM results of an Ar^+-bombarded $TiO_2(110)$ surface. (a) a LEED pattern observed with a primary energy of 54 eV, (b) a variable-current topograph (100×100 nm^2, $V_s=+2.0$ V, $I_t=0.3$ nA), and (c) a cross section determined in a constant-current scan.

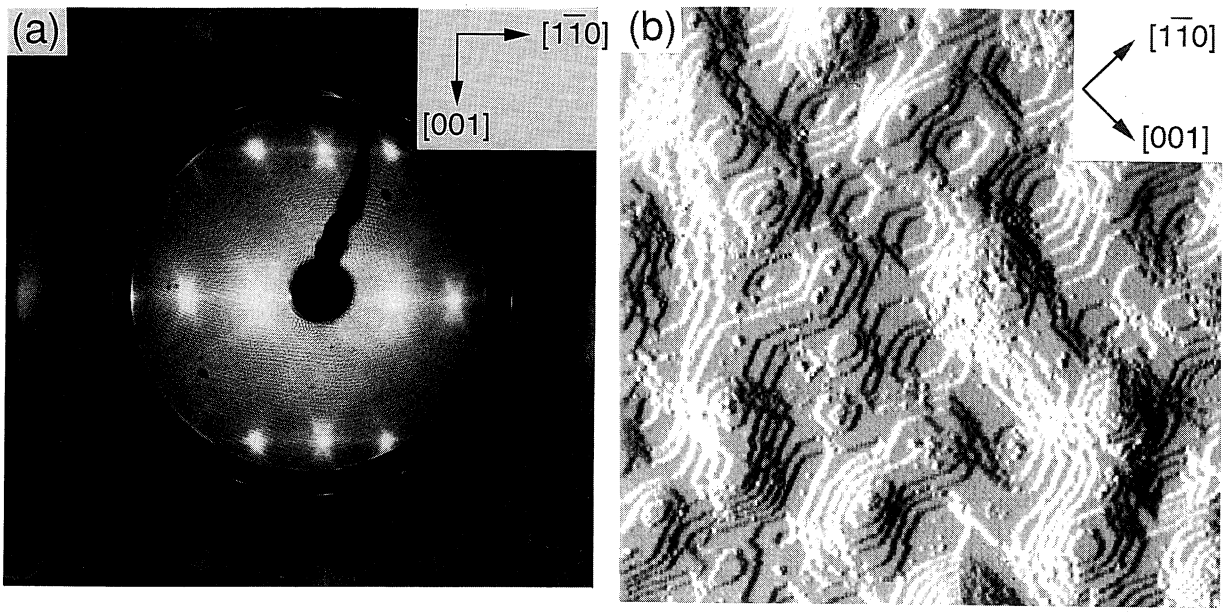

Fig. 3. LEED and STM results of the terraced $TiO_2(110)$ surface annealed at 600—800 K. (a) a LEED pattern observed on the surface annealed at 750 K with a primary energy of 48 eV, and (b) a variable-current topograph of the surface annealed at 800 K (100×100 nm^2, $V_s=+2.0$ V, $I_t=0.3$ nA).

m^{-3} had been reported for a rutile single crystal of 0.04 Ω m.[36]

The structure transformation of an Ar^+-bombarded $TiO_2(110)$ surface is mentioned in the following sections. The reconstruction of the bombarded surface was monitored with increasing temperature of vacuum annealing.

Ar^+-Bombarded $TiO_2(110)$ Surface. Figure 2 shows a LEED pattern and a variable-current topograph observed on a bombarded surface without annealing. A diffuse (1×1) pattern faintly appeared in LEED (Fig. 2a), suggesting a poorly ordered structure. The STM topograph was rugged, as shown in Fig. 2b, where corrugations were presented as if lighted from the left side. Irregular corrugations of ca. ±2 nm were observed in constant current measurements. A typical cross section is shown in Fig. 2c.

Development of (1×1) Terraces. The irregular corrugations on the bombarded surface crystallized into small and stacked terraces by vacuum annealing at 600—800 K. The terraces developed in dimension with increasing annealing temperature. Figure 3a presents the LEED pattern with broad (1×1) spots with crossed streaks recorded on a surface annealed at 750 K. The fair pattern shows that (1×1) ordered patches grew in dimension as large as the coherent length of the pri-

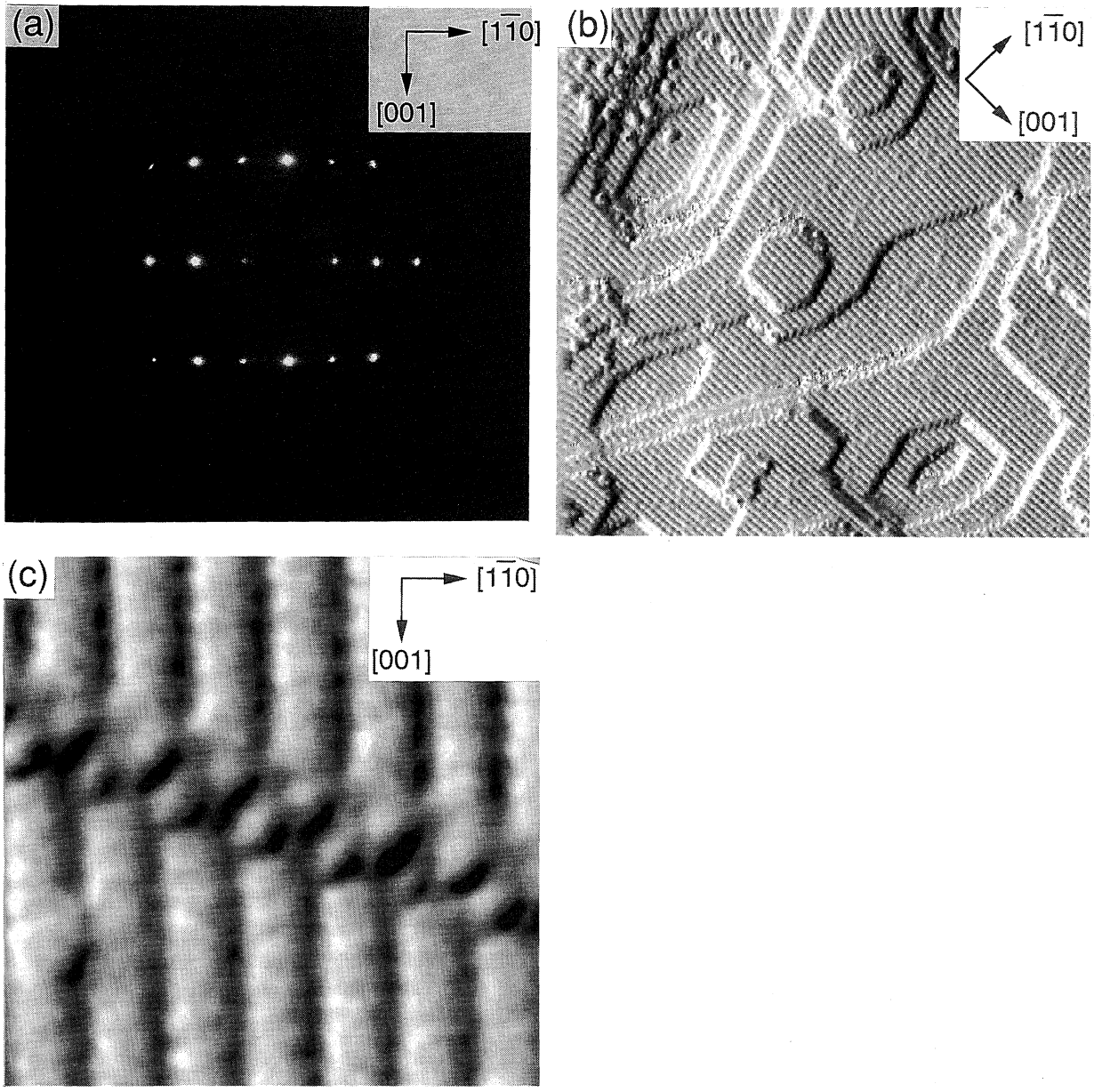

Fig. 4. LEED and STM results of the well-ordered $TiO_2(110)$-(1×1) surface annealed at 800—900 K. (a) a LEED pattern observed on the surface annealed at 880 K with a primary energy of 88 eV, (b) a variable-current topograph of the surface annealed at 860 K (100×100 nm^2, V_s=+2.0 V, I_t=0.3 nA), and (c) a variable-current topograph of stacked terraces of the surface in (b) (5×5 nm^2, V_s=+2.0 V, I_t=0.3 nA).

mary electron beam, ca. 10 nm.[37] Hexagonal terraces that were 10×10 nm^2 or smaller accordingly appeared in the topograph of Fig. 3b. The terraces were irregularly stacked and bounded by steps in the [1$\bar{1}$1] and [001] directions. The diffraction on a terrace generated the (1×1) spots, while the electron waves diffracted on the stacked terraces interfered to cause streaks normal to the azimuth of the steps. An electron-stimulated desorption (ESD) study[38] detected off-normal emissions of stimulated ions on a TiO_2(110) surface annealed at 400—800 K. Step structures parallel to the [1$\bar{1}$1] and [1$\bar{1}$3] directions were proposed for the off-normal signals.[38] Our observation partly agrees with the proposal.

The stacked terraces grew in dimension along with the annealing temperature. The crossed streaks became faint, and disappeared at 900 K. Figure 4a shows a sharp (1×1) pattern without streaks recorded on a surface annealed at 880 K. Terraces that were 30×30 nm^2 or larger were observed in a topograph on the surface annealed at 860 K (Fig. 4b). Regular ridges oriented along the [001] axis covered the surface. They were separated from each other by 0.65 nm. The separation corresponded with the (1×1) periodicity in the stoichiometric model (Fig. 1). It was thus suggested that the ridge represented the position of either the exposed Ti-row or the bridging O-row. However, it was not obvious whether the Ti-row or the O-row was imaged as the protruding ridge in the topograph.

A uniform step height (0.32 nm) was determined in constant-current measurements. This was equivalent to the layer separation of the (110) planes in a bulk crystal. Figure 4c shows an STM image for a small area over a [1$\bar{1}$1]-step, where the ridges on the adjacent terraces alternated with each other. These characteristics are well reproduced in the model shown in Fig. 5a, the situation of which is independent of the assignment of the imaged component (Ti or O). Stoichiometric truncation of the bulk and no displacement of the residual atoms are assumed in Fig. 5a. Small corrugations on the step slope observed in Fig. 4c may reflect the ions at coordinatively unsaturated positions.

The terraces observed in Figs. 3b and 4b were bounded by [1$\bar{1}$1]- and [001]-steps. The stability of those steps can be rationalized in the light of stoichiometry. A hexagonal terrace with the stable steps maintains the TiO_2 composition, if we assume Ti ions require five-fold or six-fold coordination at step edges, as illustrated in Fig. 5a where the upper terrace comprises $Ti_{69}O_{138}$. Another type of termination, e. g. a [1$\bar{1}$0]-step, leads to a composition beyond TiO_2. A rectangular terrace bounded by [1$\bar{1}$0]- and [001]-steps shown in Fig. 5b comprises $Ti_{31}O_{70}$ being out of the stoichiometry. Eight oxygen ions must be removed to maintain the TiO_2 composition. This would result in poor and hence energetically unfavorable coordination of Ti ions.

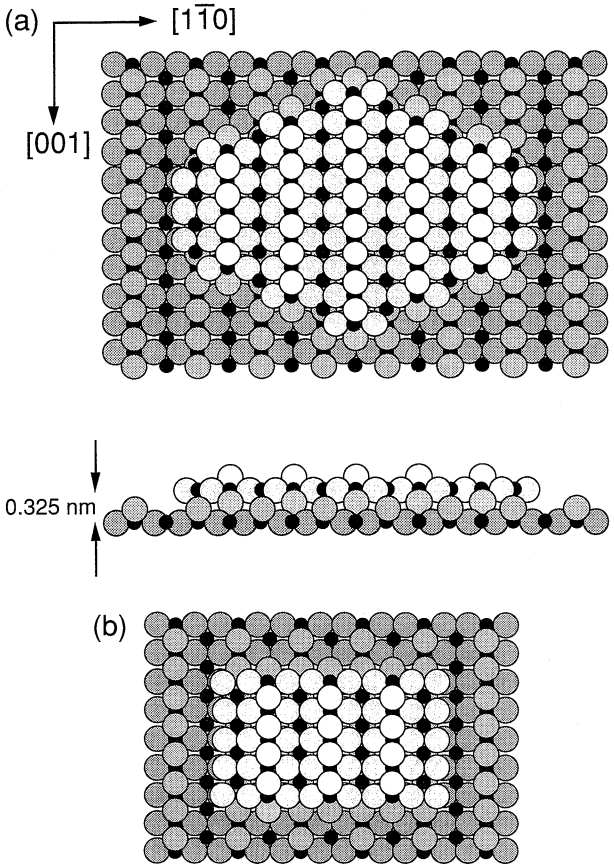

Fig. 5. (a) A model of a stacked (110)-(1×1) terrace bounded by [1$\bar{1}$1]- and [001]-steps. Plan and side views are shown. The upper terrace comprises $Ti_{69}O_{138}$ in the model, maintaining the stoichiometry. (b) Top view of a stacked (110) terrace bounded by [1$\bar{1}$0]- and [001]-steps. The upper terrace comprises $Ti_{31}O_{70}$, being out of the stoichiometry. Filled and shaded symbols represent Ti^{4+} and O^{2-}, respectively.

Ti-Row or O-Row ? It is a fundamental issue for reading topographs whether the exposed Ti-row or bridging O-row generates the protruding ridge in Fig. 4. We have already proposed that electron tunneling from the tip into the unoccupied states of the surface was responsible for the observed contrast, since the topographs were determined on a positively biased surface. The exposed five-fold coordinated Ti^{4+} ion is a reasonable source of the unoccupied states. A DV-Xα cluster calculation[39] predicted vacant 3d-states localized on the exposed Ti ion; those states could be 1—2 eV above the Fermi level, and could expand normal to the surface. These characteristics are favorable for the imaged tunneling. On the other hand, the bridging oxygen ion, the position of which is 0.15 nm closer to the tip than the Ti position in Fig. 1, may also create the observed corrugation. Finite hybridization of Ti-derived and O-derived states should be considered in this case. To examine the alternative proposition, we probed the Ti ions exposed on the (1×1) surface using imaging of individual adsorbed formate ions ($DCOO^-$).

The reaction of formic acid has been well-characterized on the $TiO_2(110)$-(1×1) surface by thermal desorption and photoelectron spectroscopy;[26] a formic acid molecule was dissociated on the surface to create an adsorbed formate anion at 300 K,

$$DCOOD + O_s^{2-} \longrightarrow DCOO^-(a) + O_sD^-(a), \quad (1)$$

where O_s^{2-} represents an oxygen anion of the substrate. The resultant formate ions were adsorbed not only on minor defect sites, but also on the (1×1) terrace. They formed an ordered (2×1)-monolayer, which was saturated at 0.5 ML. One ML is defined as the density of the (1×1) cell, 5.21×10^{18} m^{-2}. The adsorbed formate anions interacted primarily with the accessible Ti^{4+} cations due to their ionic nature. It was most unlikely that the anions were preferentially adsorbed on the oxygen ridge. Figure 6a illustrates a proposed picture of the adsorbed formate ions of the bridging configuration on the (1×1) surface.[26,40] The adsorbed formate anions, thereby, help us to probe accessible Ti cations exposed on the surface, i.e. the five-fold coordinated Ti ions. Figure 6b shows a constant-current topograph in a gray scale observed on a (110)-(1×1) surface exposed to 0.3 L (1 L=1.33×10^{-4} Pa s) DCOOD at room temperature. 97 bright spots were observed in Fig. 6b. They were assigned to individual adsorbed formate ions bridging the two adjacent Ti^{4+} atoms, because the number of the spots increased with DCOOD exposure and saturated at 0.5 ML with the (2×1) periodicity.[40] The corrugation of an isolated spot was 0.14 nm, a reasonable value for a bridging formate ion.

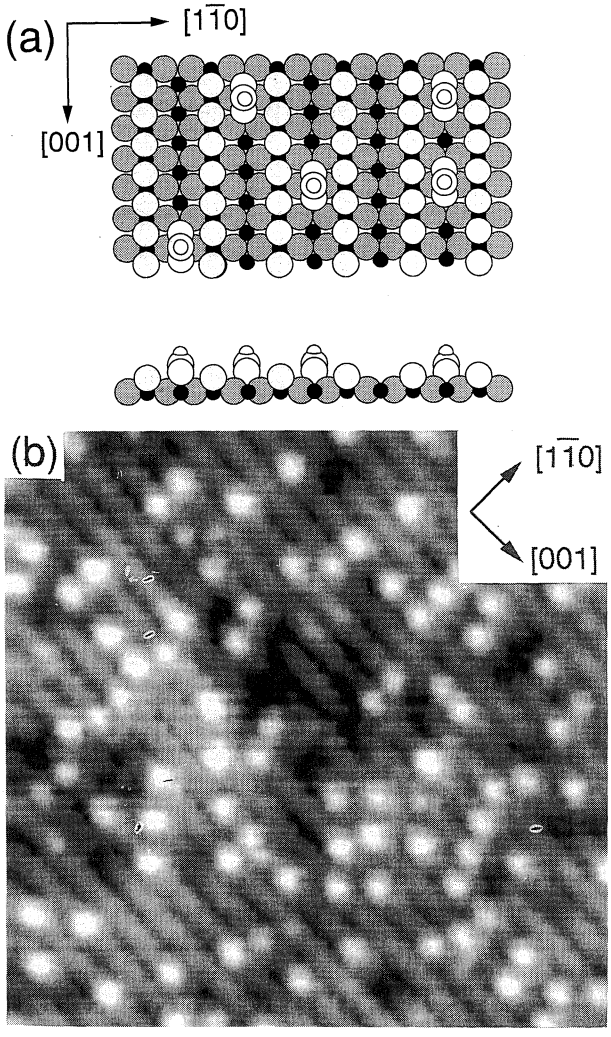

Fig. 6. (a) A model of the dispersed formate ions adsorbed on the $TiO_2(110)$-(1×1) surface.[26,40] Open symbol represents formate ions. Plan and side views are shown. (b) A constant-current image of a $TiO_2(110)$-(1×1) surface exposed to 0.3 L DCOOD at room temperature. (14×14 nm^2, V_s=+1.0 V, I_t=0.2 nA). The topography was presented in a gray scale.

Note the position of the bright spots (formate ions) relative to the substrate structure in Fig. 6b. They were always located just on the ridge of contrast. These results allowed us to conclude that the topographic ridge of the underlying (1×1) substrate represented the Ti-row of five-fold coordination. If the ridge indicated the position of the bridging O-row, the formate ions should be adsorbed between the ridges.

Atomically Resolved Corrugation on the (1×1) Surface. An atomically-resolved topograph of the (1×1) surface was observed with a smaller sample bias voltage of +1.0 V, as shown in Fig. 7. There were spots ordered in a rectangular periodicity of 0.65×0.30 nm^2. This was the size of the (1×1) unit cell, 0.649×0.296 nm^2. Hence, the spots were assigned to the individual Ti ions. The corrugation of the spots along the [001] and [1$\bar{1}$0] directions was 0.014 and 0.060 nm, respectively. These values are fairly small, and are comparable to atomic corrugations of gold surfaces (0.05—0.005

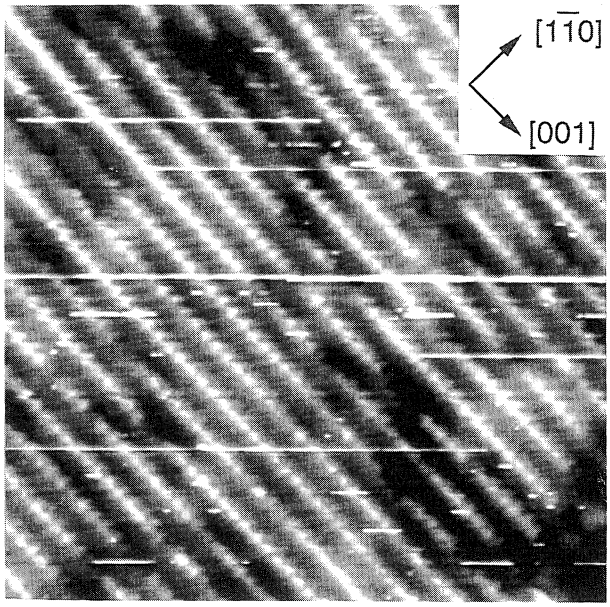

Fig. 7. A constant- current topograph of the $TiO_2(110)$-(1×1) surface. (12×12 nm^2, V_s=+1.0 V, I_t=0.3 nA). Horizontal scratches were artifacts.

nm).[41] A high spatial resolution of STM is achieved at a small tip-surface separation, i.e. at a low tunneling resistance.[42] Indeed, the atomic corrugation on metal surface is usually resolved at a low bias voltage (0.1 V or less) and at a large tunneling current (1 nA or more). The atomic resolution achieved on TiO_2(110) with a relatively high tunneling resistance can be attributed to the band structure of the substrate. Stoichiometric TiO_2 has a wide gap of 3 eV in the band structure.[43] An inverse photoemission study on TiO_2(110) found the onset of the conduction band at 1 eV above the Fermi level.[44] The tip closely approached the surface while maintaining the tunneling current when the bias voltage was reduced to +1 V.

Formation of a Double-Strand Row. Vacuum annealing at 900 K or higher temperatures caused streaks in the LEED pattern (Fig. 8a). The streaks parallel to the [1$\bar{1}$0] direction increased in intensity with the annealing temperature, and additional (1×2) spots appeared on the streaks upon annealing at 1150 K (Fig. 8b). The (1×1) periodicity was not recovered on the [1$\bar{1}$0]-streaky or (1×2) surface once reconstructed, even after re-annealing at 880 K for 1 h (Fig. 8c), though an early study reported that a (1×1) pattern was recovered on a (1×2) surface by annealing at 970 K.[34]

Responding to a transformation of the LEED pattern, we found a new feature by the STM observation, which showed wide rows parallel to the [001] axis on the (1×1) terrace. Figure 9a shows a constant-current topograph of the wide rows. The number of rows increased with the annealing temperature, and eventually covered up the surface at 1150 K accompanied by the appearance

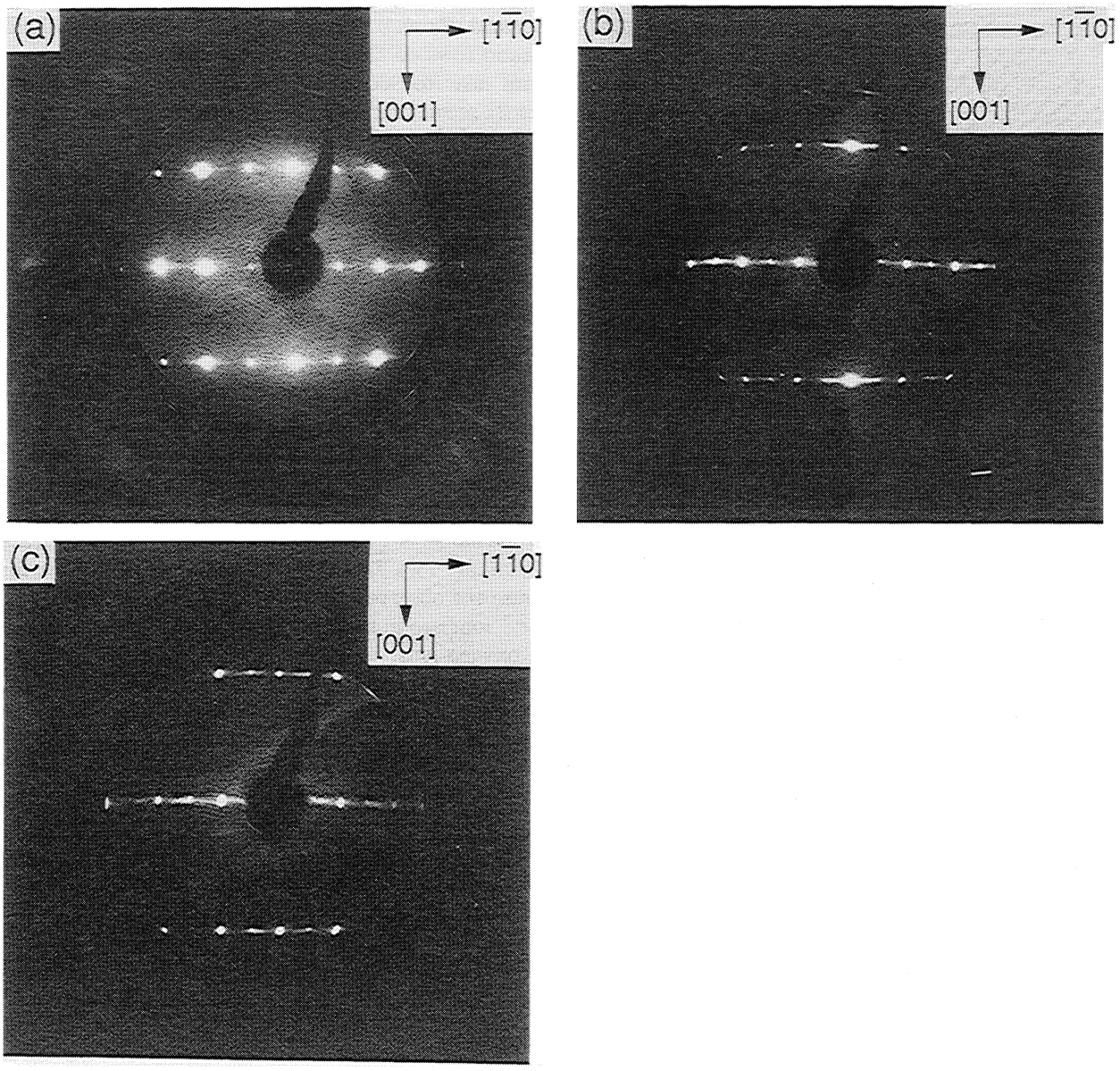

Fig. 8. LEED patterns of the TiO_2(110) surface annealed at (a) 960 and (b) 1150 K. (c) The surface in (b) was annealed again at 880 K for 1 h. (a), (b), and (c) was observed with the primary beam of 66, 54, and 65 eV, respectively.

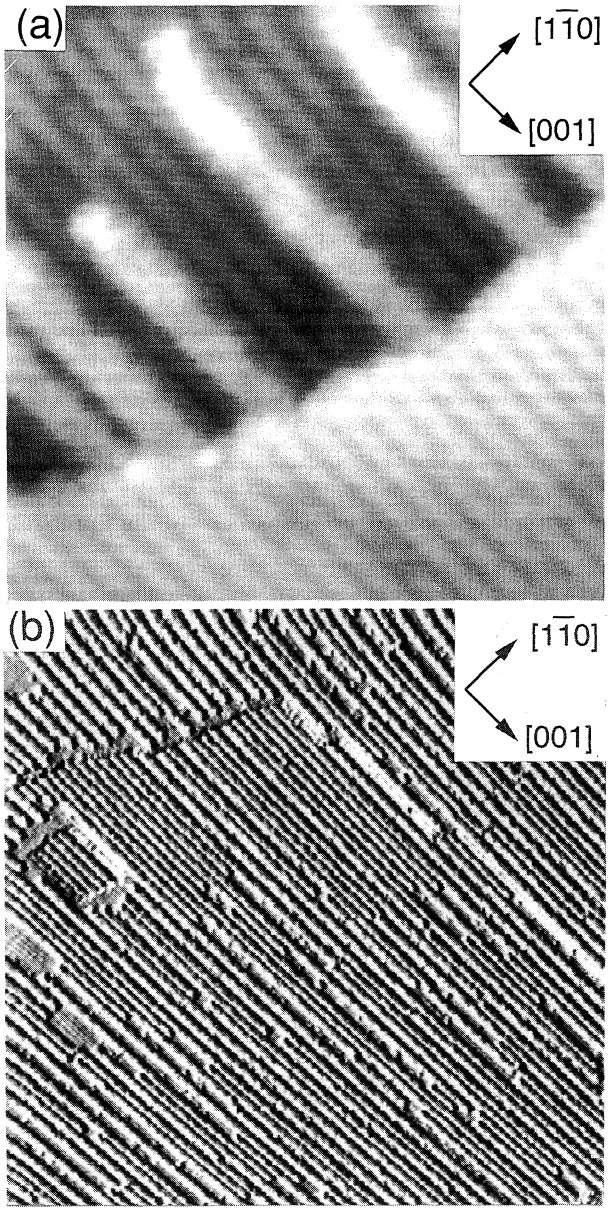

Fig. 9. STM images of double-strand rows. (a) a constant-current topograph of the rows (14×14 nm^2, V_s=+0.7 V, I_t=0.3 nA). (b) a variable-current image of the TiO_2(110)-(1×2) surface annealed at 1150 K (90×90 nm^2, V_s=+2.0 V, I_t=0.3 nA).

of the (1×2) LEED pattern. The variable-current image in Fig. 9b shows very large terraces saturated with the wide rows. Small (1×1) patches were left uncovered on the left side, indicating that the transition into the wide row structure was limited only to the top layer. The [1$\bar{1}$0]-streaks were ascribed to diffraction by rows not ordered in the [1$\bar{1}$0] direction. The [1$\bar{1}$0]-streak reflected the lack of correlation between the rows. When the surface was saturated with wide rows, they were regularly aligned on the underlying (1×1) surface, leading to the (1×2) order. The wide rows persisted on a (1×2) surface after re-annealing at 880 K, being consistent with the LEED observation.

It should be noted that each row comprised two strands separated by 0.35 nm, the separation of which was much less than that of the Ti-rows of the (1×1) surface. Hence, we hereafter designate this structure as a double-strand row. The center of the double strands was always located above a Ti-row on the underlying (1×1) surface, as shown in Fig. 9a. The height of the double-strand row was 0.20 nm, lower than a complete single step. A row was terminated by hill(s) of 0.30-nm height or by complete step(s). The diffraction patterns resulting from the rows, the [1$\bar{1}$0] streaks and the (1×2) spots, were not spread along the [001] direction at all. This showed that the double-strand row was well ordered along the row axis, though the axial corrugation could not be resolved in our measurements. The intrastructure of the double-strand row is discussed in the next section based on these characteristics.

Added Ti_2O_3 Row Model for the Double-Strand Row. Recent STM studies found double-strand rows on the TiO_2(110) surface annealed in vacuum near to 900 K, and associated the rows with a (1×2) reconstruction.[10—13] The dimensions of the reported structures agreed with ours. A (1×2) ordering on a surface heated at high temperatures had been known prior to the STM reports.[34,45] Those early works reported a decrease in the O/Ti AES intensity ratio and UPS signal from reduced Ti^{3+} species on the (1×2)-reconstructed surface. They were ascribed to oxygen release during high-temperature annealing. Hence, several models assuming a Ti-rich composition have been proposed for the double-strand row and the consequent (1×2) reconstruction.

We proposed an added Ti_2O_3 row model, as illustrated in Fig. 10a.[11] It is a reasonable assumption that added rows of partially reduced oxide form the protruding double-strand rows. The composition of a long row in the model is Ti_2O_3, leading to the 3+ charged state of titanium. Two lines of Ti^{3+} ions in an added row could cause the observed contrast of the double strands. The Ti^{3+} ions are in the optimum six-fold coordination due to oxygen ions. There are vacant octahedral sites coordinated by six O^{2-} ions in bulk rutile. The Ti^{3+} ions are assumed to move into the vacant octahedra forming the double rows, whereas oxygen ions sit on their original position. Thereby, the separation of the Ti double rows is 0.33 nm consistent with the observed value, and the height of the row becomes smaller than a complete single step. The capacity of the octahedron to coordinate a Ti^{3+} ion was suggested; Electrical conductivity measurements proposed Ti^{4+} and Ti^{3+} ions at interstitial positions in a rutile crystal reduced at 1200—1700 K.[46] The transport of Ti ions into vacant octahedra neighboring to their original sites was assumed in the formation of the crystallographic shear structures (Ti_nO_{2n-1}).[47] It was found that an Fe^{3+} ion diffused through the channels formed by the O^{2-} octahedra.[48]

Other than the added row model, three types of missing oxygen row models[10,13,34] have been proposed for

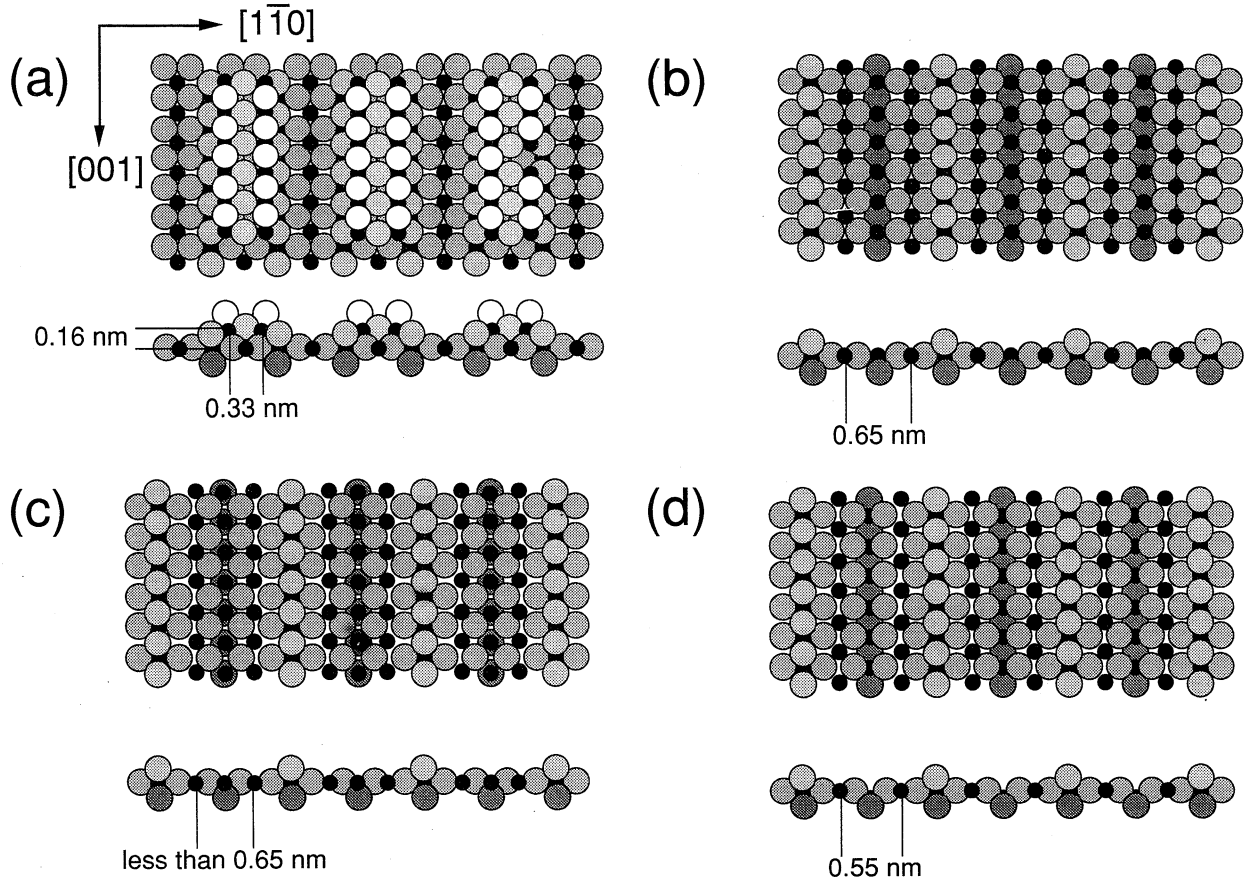

Fig. 10. Proposed models for the double-strand row on $TiO_2(110)$. (a) an added Ti_2O_3 row model,[11] (b) a simple missing oxygen row model,[34] (c) an in-plane modified missing row model,[10] and (d) an out-of-plane modified missing row model.[13] The assumed displacements are exaggerated for illustration in (c) and (d). Filled and shaded symbol represents Ti^{4+} and O^{2-}, respectively. Plan and side views are shown.

the double-strand (1×2) structure. They assumed an alternative removal of the bridging oxygen row. The original model by Wu and Møller (Fig. 10b) supposed the alternative removal of the bridging O-rows without any additional displacement of remaining atoms.[34] Sander and Engel modified the model with an in-plane transport based on their STM topographs, where the four-fold coordinated Ti ion resultant in the original model moved into a five-fold coordinated site and a pair of Ti-rows then further relaxed towards the transported Ti-row in between (Fig. 10c).[10] They assumed that the pair of relaxed Ti-rows gave rise to the double strands in STM topography. More recently, Murray et al. proposed another structure having an out-of-plane displacement; the four-fold coordinated Ti ion moved down out of its original position to relax the in-plane five-fold coordinated Ti ions (Fig. 10d).[13] The double-strand topography was ascribed to the resultant Ti-rows spaced 0.55 nm apart.

In those missing row models, the protruding double ridges observed by STM was attributed to tunneling to the states on the rows of reduced titanium ions exposed on the surface. However, the enhancement of tunneling caused by missing coordination and by reduced oxidation state seems difficult to cause the observed protrusion, as large as 0.20 nm. The surface states localized on an oxygen defect exhibited a much smaller protrusion of 0.01 nm on $SrTiO_3(100)$-$(\sqrt{5}\times\sqrt{5})$.[16] We assumed deposition of additional material instead. The adsorbed formate ion helped us again to grade the proposed models by probing titanium ions exposed on the double-strand structure. The reduced titanium ions are blocked up by oxygen ions in the added Ti_2O_3 row model, whereas other missing row models are rich in exposed Ti species accessible by adsorbed formate ions.

Figure 11 presents topographs of the double-strand rows exposed to 3 L formic acid at room temperature. We could not observe formate ions adsorbed on the rows, whereas the surrounding (1×1) area was almost saturated by formate ions in contrast (Fig. 11a). There are many double-strand rows terminated by hills in the topograph. Small spots regularly aligned over the terrace in a rectangular periodicity (0.65×0.59 nm^2) are formate ions adsorbed on (1×1) region. The spacing and dimensions of individual spots are consistent with those of the (2×1)-monolayer in a previous report.[40] However, corrugation was not observed on the rows. This indicates that the formate ions did not cover the

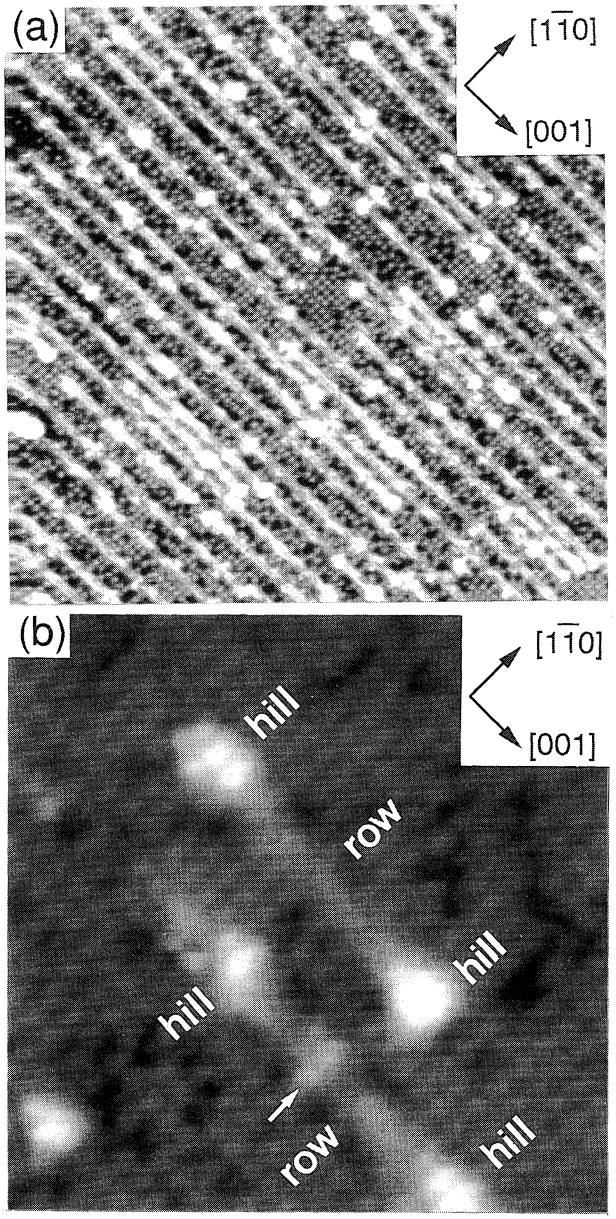

Fig. 11. Constant-current topographs of DCOOD-exposed double-strand rows on TiO_2(110). (a) a wide area (50×50 nm^2) and (b) a small area (14×14 nm^2) scans. V_s=+1.0 V, I_t=0.3 nA. Two rows and four hills are shown. A pair of formate ions adsorbed possibly on a pair of oxygen vacancies are marked by an arrow.

rows. Several formate ions were resolved on the hills and on minor defect sites on the row, as will mentioned below. It is difficult to distinguish those minor formates in Fig. 11a due to severe latitude for presentation.

The absence of formate ions covering the double-strand row strongly supports the added Ti_2O_3 row model. It was unlikely that a formate ion could not be adsorbed on the Ti ions assumed in the missing-row models. Carboxylic acid was readily dissociated to form carboxylate at room temperature with an adsorption probability near to unity on TiO_2(110)-(1×1),[26,27,40,49] faceted-TiO_2(001),[24,25] MgO(100),[50,51] NiO(100)-film,[52] ZrO_2(100),[53] Cu_2O-(100),[54] SnO_2(110),[55] nonpolar ZnO(10$\bar{1}$0),[56] and Zn-polar ZnO(0001).[57] The only metal-oxide surface disabled from carboxylic acid dissociation is the O-polar ZnO(000$\bar{1}$) truncation. The inability was attributed to the absence of accessible cation–anion site pairs on the O-polar surface.[58] Hence, the observed inability of formate adsorption indicates the absence of Ti ions exposed on the double-strand structure. It was also less possible that the formate ions adsorbed on Ti ions assumed in the missing row models were invisible to STM. The height of the rows gave no change upon exposure to formic acid.

Figure 11b shows a topograph for a small area including DCOOD-exposed two double-strand rows terminated by hills. A pair of small spots (marked by an arrow) were observed on a row. They were probably formates adsorbed on Ti sites created by oxygen defects. Formate ions of the (2×1) order, which were presented by spots of intermediate contrast, covered the (1×1) area surrounding the rows. Topographic measurements showed that the marked formate ions were located at a higher z-position by 0.1 nm than those adsorbed on the underlying (1×1) region. This also supports our model with the Ti^{3+} ions lifted up in the added row. A lift of 0.16 nm was estimated in the model (Fig. 10a), assuming ideal octahedra channels. We thus conclude the added Ti_2O_3 row structure. Brighter spots on the hills were also ascribed to adsorbed formates, since they were not observed in a pre-exposure measurement. The formates indicate accessible Ti ions left on the hills. Figure 12 shows an extended added-row model terminated by a hill and a complete terrace, on the basis of the topograph. Possible sites for formate adsorption are marked by an ellipse on the row and the hill.

The added Ti_2O_3 row is a new and highly anisotropic surface-limited phase of titanium oxide that is different from the known compounds, Ti_2O, TiO, Ti_2O_3, Ti_3O_5, TiO_2, and a series of partially reduced oxide of crystallographic shear structures, Ti_nO_{2n-1} (n=4—10). The reconstructions of TiO_2 surfaces have been always related to oxygen vacancies created by high-temperature annealing, assuming Ti ions of reduced coordination at the original positions,[23] though interstitial Ti ions were proposed in interpretation of bulk conductivity.[46] In the added row, reduced Ti^{3+} ions are located at the center of the oxygen octahedra having an optimum six-fold coordination. Hence, it is reasonable to assume that optimizing coordination drives the Ti^{3+} ions to the octahedra channel. It was pointed out that Ti ions moved into unoccupied octahedra in the initial stage of shear-structure formation.[47] These arguments suggest the role of interstitial Ti ions at least as important as that of oxygen vacancies on TiO_2 surfaces. The present study also demonstrates that probing experiments with an adsorbed molecule help us to characterize an imaged site on multi-component materials, e. g. metal oxide,

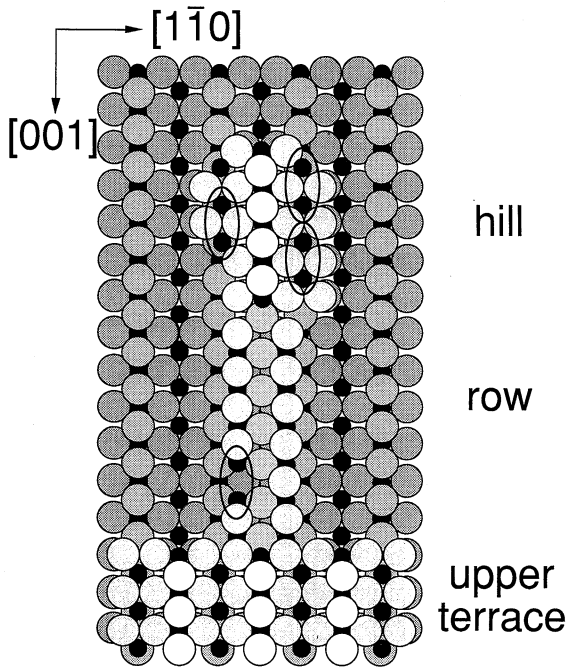

Fig. 12. An extended model of the added Ti_2O_3 row. Possible sites for formate adsorption are marked by an ellipse.

the chemical nature of which site is not always obvious by STM topography alone.

Conclusions

The atomic-scale structures of the TiO_2(110) surface were determined by STM and LEED with increasing temperature during vacuum annealing. The irregular corrugations on an Ar^+-bombarded surface crystallized into stacked (1×1) terraces upon annealing at 600—800 K. The terraces developed in dimension as large as 30×30 nm^2, being annealed at 900 K. Regular ridges along the [001]-axis were observed on the terrace, and assigned to the one-dimensional rows of five-fold coordinated Ti^{4+} ions. The position of the Ti^{4+} ions was probed by imaging adsorbed formate ions. The individual Ti^{4+} ions were resolved corresponding with the (1×1) periodicity. Annealing at higher temperatures resulted in the formation of wide protruding rows comprising double strands. Probing experiments with adsorbed formate ions allowed us to conclude an added Ti_2O_3 row model for that structure, which is a new surface-limited phase of titanium oxide. These results demonstrate the ability of a probing experiment with an adsorbed molecule to determine the chemical nature of imaged sites on multi-component materials by STM.

References

1) H.-J. Güntherodt and R. Wiesendanger, "Scanning Tunneling Microscopy I," 2nd ed, Springer-Verlag, Berlin (1994).

2) R. Wiesendanger, "Scanning Probe Microscopy and Spectroscopy," Cambridge University Press, Cambridge (1994).

3) T. A. Land, T. Michely, R. J. Behm, J. C. Hemminer, and G. Comsa, *J. Chem. Phys.*, **97**, 6774 (1992).

4) L. P. Nielsen, F. Besenbacher, E. Lægsgaard, and I. Stensgaard, *Phys. Rev. B*, **44**, 13156 (1991).

5) Y. Kuk, F. M. Chua, P. J. Silverman, and J. A. Meyer, *Phys. Rev. B*, **41**, 12393 (1990).

6) A. Feltz, U. Memmert, and R. J. Behm, *Surf. Sci.*, **314**, 34 (1994).

7) G. S. Rohrer, V. E. Henrich, and D. A. Bonnell, *Science*, **250**, 1239 (1990).

8) G. S. Rohrer, V. E. Henrich, and D. A. Bonnell, *Surf. Sci.*, **278**, 146 (1992).

9) Q. Zhong, J. M. Vohs, and D. A. Bonnell, *Mater. Res. Soc. Symp. Proc.*, **237**, 453 (1992).

10) M. Sander and T. Engel, *Surf. Sci. Lett.*, **302**, L263 (1994).

11) H. Onishi and Y. Iwasawa, *Surf. Sci. Lett.*, **313**, L783 (1994).

12) D. Novak, E. Garfunkel, and T. Gustafsson, *Phys. Rev. B*, **50**, 5000 (1994).

13) P. W. Murrey, N. G. Condon, and G. Thornton, *Phys. Rev. B*, **51**, 10989 (1995).

14) P. W. Murray, F. M. Leibsle, H. J. Fisher, C. F. J. Flipse, C. A. Muryn, and G. Thornton, *Phys. Rev. B*, **46**, 12877 (1992).

15) T. Matsumoto, H. Tanaka, T. Kawai, and S. Kawai, *Surf. Sci. Lett.*, **278**, L153 (1992).

16) H. Tanaka, T. Matsumoto, T. Kawai, and S. Kawai, *Jpn. J. Appl. Phys.*, **32**, 1405 (1993).

17) G. Tarrach, D. Bürgler, T. Schaub, R. Wiesendanger, and H.-J. Güntherodt, *Surf. Sci.*, **285**, 1 (1993).

18) W. Lu, N. Nevins, M. L. Norton, and G. S. Rohrer, *Surf. Sci.*, **291**, 395 (1993).

19) G. S. Rohrer, W. Lu, R. L. Smith, and A. Hutchinson, *Surf. Sci.*, **292**, 261 (1993).

20) T. Oshio, Y. Sakai, T. Moriya, and S. Ehara, *Scanning Microsc.*, **7**, 33 (1993).

21) R. L. Smith, W. Lu, and G. S. Rohrer, *Surf. Sci.*, **322**, 293 (1995).

22) H. C. Galloway, J. J. Benítez, and M. Salmeron, *J. Vac. Sci. Thechnol., A*, **12**, 2302 (1994).

23) V. E. Henrich, and P. A. Cox, "The Surface Science of Metal Oxides," Cambridge University Press, Cambridge (1994).

24) K. S. Kim and M. A. Barteau, *J. Catal.*, **125**, 353 (1990).

25) K. S. Kim and M. A. Barteau, *Langmuir*, **6**, 1485 (1990).

26) H. Onishi, T. Aruga, and Y. Iwasawa, *J. Catal.*, **146**, 557 (1994).

27) H. Onishi, T. Aruga, and Y. Iwasawa, *J. Am. Chem. Soc.*, **115**, 10460 (1993).

28) L. E. Firment, *Surf. Sci.*, **116**, 205 (1982).

29) P. Zschck, J. B. Cohen, and Y. W. Chung, *Surf. Sci.*, **262**, 395 (1992).

30) V. E. Henrich and R. L. Kurtz, *Phys. Rev. B*, **23**, 6280 (1981).

31) B. L. Maschhoff, J.-M. Pan, and T. E. Madey, *Surf. Sci.*, **259**, 190 (1991).

32) H. Onishi and Y. Iwasawa, *Langmuir*, **10**, 4414

(1994).
33) K. Sakamaki, K. Itoh, A. Fujishima, and Y. Gohshi, *J. Vac. Soc. Technol.*, **8**, 614 (1990).
34) P. J. Møller and M.-C. Wu, *Surf. Sci.*, **224**, 265 (1989).
35) H. Onishi and Y. Iwasawa, *Jpn. J. Appl. Phys.*, **33**, L1338 (1994).
36) R. G. Breckenridge and W. R. Hosler, *Phys. Rev.*, **91**, 793 (1953).
37) G. Ertl and J. Küppers, "Low Energy Electrons and Surface Chemistry," Verlag, Weinheim (1974), pp. 159—160.
38) R. L. Kurtz, *Surf. Sci.*, **177**, 526 (1986).
39) M. Tsukada, C. Satoko, and H. Adachi, *J. Phys. Soc. Jpn.*, **45**, 1610 (1979).
40) H. Onishi and Y. Iwasawa, *Chem. Phys. Lett.*, **226**, 111 (1994).
41) Y. Kuk, P. J. Silverman, and H. Q. Nguyen, *J. Vac. Sci. Technol., A*, **6**, 524 (1988).
42) Ref. 2, p. 124.
43) F. A. Grant, *Rev. Mod. Phys.*, **31**, 646 (1959).
44) A. E. Taverner, P. C. Hollamby, P. S. Aldridge, and R. G. Egdell, *Surf. Sci.*, **287/288**, 653 (1993).
45) C. C. Lo, S. C. Tsai, M. K. Bahl, and Y. W. Chung, *Surf. Sci.*, **95**, 1 (1980).
46) P. Kofstad, *J. Less Common Met.*, **13**, 635 (1967).
47) S. Andersson and A. D. Wadsley, *Nature*, **211**, 581 (1966).
48) J. L. Steele and E. R. McCartney, *Nature*, **222**, 79 (1969).
49) H. Onishi, T. Aruga, C. Egawa, and Y. Iwasawa, *Surf. Sci.*, **193**, 33 (1988).
50) H. Onishi, C. Egawa, T. Aruga, and Y. Iwasawa, *Surf. Sci.*, **191**, 479 (1987).
51) X. D. Peng and M. A. Barteau, *Catal. Lett.*, **7**, 395 (1990).
52) C. M. Truong, M.-C. Wu, and D. W. Goodman, *J. Chem. Phys.*, **97**, 9447 (1992).
53) P. A. Dilara and J. M. Vohs, *J. Phys. Chem.*, **97**, 12919 (1993).
54) K. H. Schulz and D. F. Cox, *J. Phys. Chem.*, **96**, 7394 (1992).
55) V. A. Gercher and D. F. Cox, *Surf. Sci.*, **312**, 106 (1994).
56) S. Akhter, K. Lui, and H. H. Kung, *J. Phys. Chem.*, **89**, 1958 (1985).
57) J. M. Vohs and M. A. Barteau, *Surf. Sci.*, **176**, 91 (1986).
58) J. M. Vohs and M. A. Barteau, *Surf. Sci.*, **201**, 481 (1988).